A Robust Control Scheme Based on ISMC for the Brushless Doubly Fed Induction Machine

Guanguan Zhang, Jian Yang, *Member, IEEE*, Yao Sun, *Member, IEEE*, Mei Su, Weiyi Tang, Qi Zhu, and Hui Wang

***Abstract*—The brushless doubly fed induction machine (BDFM) has great potential in the wind energy generation system because it offers the advantages of higher reliability and maintenance-free operation. In this paper, a mathematical model in the power windings stator flux orientation frame is discussed by taking the rotor flux as the disturbance. Consequently, the control of the BDFM system is implemented by generating suitable control winding currents. Moreover, in order to eliminate the speed error and compensate the system uncertainties caused by the rotor flux and parameter perturbations, an integral sliding mode variable structure controller for the rotor speed is developed, and the reactive power is adjusted by a proportional-integral (PI) controller in the outer-loop. Furthermore, the control winding currents are regulated by the PI control scheme in the inner-loop. The proposed control frame achieves a good static and satisfactory dynamic control performance. Finally, simulation and experimental results are used to verify the correctness and feasibility of the proposed method.**

***Index Terms*—Brushless doubly fed induction machine (BDFM), integral sliding mode control (ISMC).**

NOMENCLATURE

φ, v, i	Flux, voltage, and current.
R, L	Winding resistance and self-inductance.
M, L_1	Mutual inductance and leakage inductance.
T_e, T_L	Electromagnetic torque and load torque.
p	Number of pole pairs.
ω	Angular frequency.
θ_p, θ_r	Unified reference frame position in PW and mechanical rotor-shaft angular position.
δ_p, δ_c	Initial mechanical rotor-shaft angular position related to the p_p -type pole-pair distribution and p_c-type pole-pair distribution.
$Im[x]$	Imaginary part of x.
J, B	Inertia constant of the system and the friction coefficient of the motor.

SUBSCRIPTS

p, c, r	Power winding (PW), control winding (CW), and rotor winding.
pd, pq	dq components of PW variables.
cd, cq	dq components of CW variables.
ref	Reference value.
0	Nominal value of the corresponding parameters.

SUPERSCRIPT

$*$	Conjugate.
$\rightarrow$	Vector form.
p, c	PW reference frame and CW reference frame.
rp	Rotor reference frame in a p_p -type pole-pair distribution.
rc	Rotor reference frame in a p_c -type pole-pair distribution.
dq	Rotating PW flux frame.

Manuscript received July 26, 2016; revised November 28, 2016 and March 21, 2017; accepted May 15, 2017. Date of publication May 26, 2017; date of current version January 3, 2018. This work was supported in part by the National Natural Science Foundation of China under Grant 61622311, in part by Natural Science Foundation of Hunan Province of China under Grant 2016JJ1019, in part by Key Scientific and Technological Plan Project of Hunan Province under Grant 2016GK2039, in part by the Fundamental Research Funds for the Central Universities of Central South University under Grant 2015zzts057, and in part by the Project of Innovation-Driven Plan in Central South University. Recommended for publication by Associate Editor F. W. Fuchs. *(Corresponding author: Jian Yang.)*

The authors are with the School of Information Science and Engineering, Central South University, Changsha 410083, China (e-mail: dr_zgg@163.com; jian.yang@csu.edu.cn; yaosun@csu.edu.cn; sumeicsu@mail.csu.edu.cn; 154601016@csu.edu.cn; zhu_qi@csu.edu.cn; wanghuicp9@csu.edu.cn).

Color versions of one or more of the figures in this paper are available online at http://ieeexplore.ieee.org.

Digital Object Identifier 10.1109/TPEL.2017.2708741

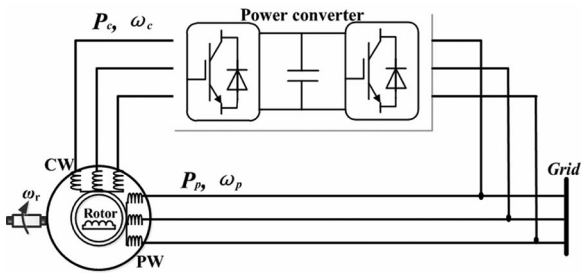

Fig. 1. Basic structure of the BDFM system.

I. INTRODUCTION

BRUSHLESS doubly fed machines (BDFMs) inherit the merits of doubly fed induction machines (DFIMs), such as small converter capacities (e.g., approximately 30% of the machine rating), low withstand voltages of the switching devices, adjustable speeds and power factors, and so on [1]. Moreover, BDFMs eliminate the slip rings and electrobrushes so as to achieve higher reliability and maintenance-free operation [2]. They, therefore, have great potential applications in wind energy generation system and adjustable speed drive system [3]–[5].

As shown in Fig. 1, the BDFM has two stator windings, denoted as power winding (PW) and control winding (CW). The PW stator is directly connected to the power grid, and the CW stator is connected to a bidirectional power converter. The rotor

winding is specially designed, and the CW stator can modify and control the rotor current that is induced by the PW stator. The electromagnetic torque and reactive power of the BDFM are coupled with the two stator currents and the rotor current, but only the CW stator is directly controlled by the converter. As a consequence, the difficulty in controlling the BDFM increases. The control issue has attracted great attention in the study of the BDFM, and several control strategies [6]–[22] have been proposed.

The scalar control is implemented by controlling the angular frequency and stator current amplitude of CW [6], which is first used to control the BDFM system. Then, the open-loop voltage control [7], which is similar to the V/F control of induction motors, and the closed loop scalar current control [8] are proposed. Based on the electromagnetic torque equation in [9], the mechanism of scalar control is illustrated in [10]. Referring to the power control in the electric power system, the electromagnetic torque is regulated by the phase angle of the CW stator voltage, and the reactive power is affected by the amplitude of the CW stator voltage. The closed-loop current control for the stand-alone mode is drawn into the scalar control in [11]. Furthermore, because the scalar control depends on the static analysis of the BDFM, it is only suitable for industrial applications with low-performance requirements, such as pumps or fan drives.

In addition, the direct torque control (DTC) [12], [13] and vector control methods as the mainstream control schemes, have been widely utilized in the BDFM system. Moreover, because of the complex structure, a complete decoupling control and good control performance are difficult to achieve for a BDFM. In [12], a DTC strategy with proportional-integral (PI) regulator loops is proposed. However, using pulse width modulation (PWM) modulators does not take advantage of the features of DTC strategies to obtain high dynamic responses. A classical DTC strategy is then developed for the BDFM in [13]; however, only the electromagnetic torque or the CW stator flux can be controlled in some sectors. In addition to the methods mentioned above, an indirect stator-quantities control, derived from DTC, is proposed in [14]. Moreover, it is implemented in the unified $\alpha\beta$ reference frame oriented on the CW of the BDFM. In conclusion, the DTC methods need to calculate electromagnetic torque and estimate CW flux in each sampling period, both of which are relatively complex.

In terms of vector control methods [15]–[22], several strategies based on different flux orientation frames are discussed. However, because the amplitude of rotor flux is small, the rotor flux oriented control method in [16] and the combined magnetizing flux oriented control in [17] are difficult to implement in practical applications. In contrast, the stator-flux-oriented control methods are more feasible. A simple control method without inner-loop controllers is discussed in [18]; it compensates all of the cross-perturbation terms by feed forward control, but the system dynamic performance is poor. Based on the unified reference frame vector model proposed in [19], a cascaded double closed-loops control method is proposed in [20] and is adopted in [21] for a matrix converter-fed BDFM system. In order to adapt to the unbalanced gird, the PI controller is replaced by a PI resonant (PIR) controller in [22]. Although the dynamic control performance is guaranteed by this method, the decoupling process is very tedious in the control system.

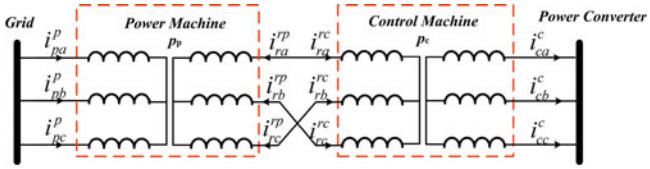

Fig. 2. Simplified schematic diagram of the BDFM windings.

In this paper, the rotor flux is taken as a disturbance, and an effective control scheme is developed in the PW stator flux orientation frame. In the proposed method, in order to guarantee the system tracking performance and eliminate the speed error caused by system uncertainties, speed tracking is realized by the integral sliding mode control (ISMC) method, and the reactive power is adjusted by a PI controller. For the inner-loop, the PI control scheme is utilized. Finally, a good control performance is verified using the BDFM experimental platform.

II. Mathematical Model of the BDFM

A. Unified Reference Frame Model

In order to conveniently design the controller, a mathematical model of the BDFM, based on the space vector representations, is given. As a self-cascaded machine, the BDFM design concept is derived from the cascaded connection of winding induction machines with a common shaft [23], and the mathematical model of the BDFM can be deduced from the inverse coupling mode of the cascaded-induction motor [24].

The simplified schematic diagram of BDFM windings is shown in Fig. 2, and the directions of the two stator currents and the rotor current are given. The relationship of the two rotor variables is expressed as

$$\vec{v}_r^{\,rp} = (\vec{v}_r^{\,rc})^*, \quad \vec{i}_p^{\,rp} = -\left(\vec{i}_r^{\,rc}\right)^*. \tag{1}$$

Referring to the induction motor, the stator voltage and flux equations are in the respective reference frames, whereas the rotor equations are in the *rp* reference frame. The mathematical model of the BDFM is then written as

$$\vec{v}_p^{\,p} = R_p\vec{i}_p^{\,p} + \frac{d\vec{\varphi}_p^{\,p}}{dt}, \quad \vec{\varphi}_p^{\,p} = L_p\vec{i}_p^{\,p} + M_p\left(e^{jp_p(\theta_r+\delta_p)}\vec{i}_r^{\,rp}\right) \tag{2}$$

$$\vec{v}_c^{\,c} = -R_c\vec{i}_c^{\,c} + \frac{d\vec{\varphi}_c^{\,c}}{dt}, \quad \vec{\varphi}_c^{\,c} = -L_c\vec{i}_c^{\,c} + M_c\left(e^{jp_c(\theta_r+\delta_c)}\vec{i}_r^{\,rc}\right) \tag{3}$$

$$0 = R_r\vec{i}_r^{\,rp} + \frac{d\vec{\varphi}_r^{\,rp}}{dt},$$

$$\vec{\varphi}_r^{\,rp} = L_r\vec{i}_r^{\,rp} + M_p\left(e^{-jp_p(\theta_r+\delta_p)}\vec{i}_p^{\,p}\right) + M_c\left(e^{-jp_c(\theta_r+\delta_c)}\left(\vec{i}_c^{\,c}\right)^*\right) \tag{4}$$

where $R_r = R_{r1} + R_{r2}$, $L_r = L_{r1} + L_{r2}$, and R_{r1}, R_{r2}, L_{r1}, and L_{r2}, are the rotor resistance and inductance of the power machine and control machine, respectively.

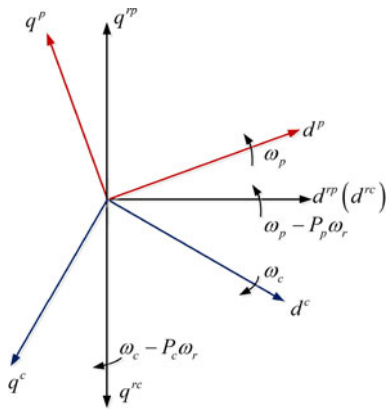

Fig. 3. Vector diagram of the BDFM reference frames.

B. A dq Model in the PW Reference Frame

As shown in (2)–(4), the mathematical model refers to three different frames, and two pole-pair distributions are considered. It is, therefore, not suitable for system analysis. The vector diagram of BDFM reference frames, synchronous with PW and CW stator frequencies, is shown in Fig. 3. The electrical variables of the *rp* frame and the *rc* frame are in the opposite sequence, and the transformation relations between the *p* reference frame, the *rp* reference frame and the *c* reference frame, are given as

$$\begin{aligned}\vec{x}_c^p &= e^{j\left(p_p\left(\theta_r+\delta_p\right)+p_c\left(\theta_r+\delta_c\right)\right)}\left(\vec{x}_c^c\right)^* \\ \vec{x}_r^p &= e^{jp_p\left(\theta_r+\delta_p\right)}\vec{x}_{rp}^{rp}.\end{aligned} \tag{5}$$

Denoting the stator PW reference frame as the overall static reference frame, a *dq* reference frame with a p_p -type pole-pair distribution is developed by $\vec{x}^{dq} = e^{-j\theta_p}\vec{x}^p$, and then a *dq* BDFM reference model is obtained. Taking $v_c = -\vec{v}_c^{dq}$ and $\varphi_c = -\vec{\varphi}_c^{dq}$, and removing the vector and *dq* notations in order to simplify the expressions, the BDFM mathematical model is expressed as

$$v_p = R_p i_p + \frac{d\varphi_p}{dt} + j\omega_p\varphi_p \tag{6}$$

$$\varphi_p = L_p i_p + M_p i_r \tag{7}$$

$$v_c = R_c i_c + \frac{d\varphi_c}{dt} + j\left(\omega_p - \left(p_p + p_c\right)\omega_r\right)\varphi_c \tag{8}$$

$$\varphi_c = L_c i_c + M_c i_r \tag{9}$$

$$0 = R_r i_r + \frac{d\varphi_r}{dt} + j\omega_{rp}\varphi_r \tag{10}$$

$$\varphi_r = L_r i_r + M_p i_p + M_c i_c \tag{11}$$

where $\omega_p = d\theta_p/dt$, $\omega_r = d\theta_r/dt$, and $\omega_{rp} = \omega_p - p_p\omega_r$.

The electromagnetic torque of the BDFM is also calculated according to the inverse coupling mode of the cascaded-induction motor, and it can be expressed as

$$\begin{aligned}T_e &= T_{ep} + T_{ec} \\ &= \frac{3}{2}p_p\mathrm{Im}\left[\left(\varphi_p\right)^* \cdot i_p\right] + \frac{3}{2}p_c\mathrm{Im}\left[\varphi_c \cdot \left(i_c\right)^*\right].\end{aligned} \tag{12}$$

The mechanical equation of the BDFM is then identical to that of the induction motor, and it is written as

$$J\frac{d\omega_r}{dt} = T_e - B\omega_r - T_L. \tag{13}$$

As shown in (6)–(13), the BDFM model is more complex than the DFIM model. The rotor flux in (11) is related to the two stator currents and the rotor current. The electromagnetic torque is determined by two components: one is produced by the PW stator, and the other is generated via the flux and stator current of the CW stator. Clearly, these variables are strongly coupled and quite nonlinear, and the interaction of these variables is complex. In this case, control schemes are difficult to design. Thus, modified mathematical models of the electromagnetic torque and reactive power are discussed next, in order to facilitate the controller design.

C. Electromagnetic Torque and Reactive Power in a PW Stator Flux Orientation Frame

For simplicity, a PW flux orientation is developed as $\varphi_{pd} = |\varphi_p|$, $\varphi_{pq} = 0$. By ignoring the PW stator resistance R_p, the PW stator voltage is written as $v_{pd} = 0$, $v_{pq} = |v_p|$. When the grid is balanced and strong, the frequency and amplitude of φ_p is quasi-constant. According to PW stator voltage (6), φ_p can be simply calculated as $\varphi_p = v_p e^{-j\frac{\pi}{2}}/\omega_p$ by ignoring the PW stator resistance, where v_p is obtained by sampling the grid voltage and using the phase lock loop method. However, when the grid is weak, the voltage-model-based estimator is built to obtain φ_p [25], and is achieved by the modified integral of $(v_p - R_p i_p)$, with the measured stator current and stator voltage. This method is utilized in this paper by considering the voltage fluctuation of the practical grid.

In the PW stator flux orientation frame, the electromagnetic torque in (12) is represented by the PW stator flux φ_p, the rotor flux φ_r, and the CW stator current i_c, and it is expressed as

$$T_e = \frac{3M_pM_c\left(p_p + p_c\right)|\varphi_p|}{2\left(L_pL_r - {M_p}^2\right)}i_{cq} - \frac{3M_p\left(p_p+p_c\right)}{2\left(L_rL_p-{M_p}^2\right)}|\varphi_p|\,\varphi_{\mathrm{rq}}. \tag{14}$$

Similarly, the reactive power of the BDFM PW stator is expressed as

$$\begin{aligned}Q_p &= \frac{3}{2}\mathrm{Im}\left[v_p \cdot \left(i_p\right)^*\right] \\ &= \frac{3\,|v_p|}{2\left(L_rL_p-{M_p}^2\right)}\left(L_r\,|\varphi_p| + M_pM_ci_{cd} - M_p\varphi_{\mathrm{rd}}\right).\end{aligned} \tag{15}$$

Furthermore, because the PW stator of the BDFM is directly connected to the power grid, the stator voltage v_p and PW stator flux φ_p are clamped to some extent. It can be seen from (14) and (15) that T_e and Q_p mainly depend on the CW stator current i_c when the effects of φ_r are negligible. As a result, controlling electromagnetic torque and reactive power is achieved by generating a proper i_c, and the control difficulty is correspondingly reduced. As discussed in [26], the rotor flux is considered as zero when the speed of the BDFM is in the range of $\pm 30\%$ around the natural speed. However, the rotor flux cannot be

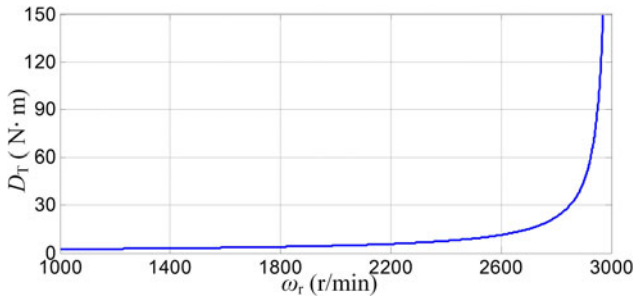

Fig. 4. Effect of φ_r on T_e with different rotor speeds.

directly ignored under other working conditions. Thus, the effects of the rotor flux are taken into consideration when designing the control scheme in this paper, and the effects of φ_r on the control system are discussed next.

D. Effects of the Rotor Flux on the Electromagnetic Torque

From (7), (9)–(11), the rotor flux can be expressed by φ_p and i_c, which is written as

$$\frac{d\varphi_r}{dt} = -\frac{R_r L_p \varphi_r}{\left(L_r L_p - {M_p}^2\right)} - j\omega_{\rm rp}\varphi_r + \frac{R_r M_p}{\left(L_r L_p - {M_p}^2\right)}\varphi_p + \frac{R_r L_p M_c}{\left(L_r L_p - {M_p}^2\right)} i_c. \quad (16)$$

In (16), φ_r is the zero dynamics by assuming i_c is in the steady state, because φ_p and i_c are constant and bounded. In this case, φ_r can automatically reach a steady state because the coefficient of φ_r is negative. Consequently, φ_r is stable without control.

A stationary solution of φ_r is then obtained by setting the differential terms of (6), (8), and (10) to zero, and it is expressed as

$$\varphi_r = \frac{-R_r\left(R_p\varphi_p - L_p v_p + j\omega_p L_p \varphi_p\right)}{jM_p R_p \omega_{rp}}. \quad (17)$$

From (17), φ_r is approximately equal to $-R_r\varphi_p/(j\omega_{rp}M_p)$, by assuming $v_p = j\omega_{\rm p}\varphi_p$, and $\varphi_{rd} = 0$, $\varphi_{rq} = R_r\varphi_{pd}/(\omega_{rp}M_p)$. Clearly, φ_r mainly affects the electromagnetic torque, and its effects on the reactive power are almost zero. Moreover, a control scheme is designed according to (14). The effect of φ_r on T_e is defined as D_T, which is calculated by (14) and (17) as

$$D_T = \frac{3M_p\left(p_p+p_c\right)}{2\left(L_r L_p - {M_p}^2\right)}\left|\varphi_p\right|\varphi_{\rm rq} = \frac{3\left(p_p+p_c\right)R_r\left|\varphi_p\right|^2}{2\left(L_r L_p - {M_p}^2\right)\omega_{\rm rp}}. \quad (18)$$

It can be seen that D_T increases with a rise in rotor speed. Moreover, it is negligible at low rotor speeds, and the BDFM system is simplified to a conventional DFIM system. In addition, the conventional control schemes of DFIM are effective. However, when ω_r increases to a high value, φ_r increases rapidly, and D_T becomes significant. In order to intuitively show the relationship between D_T and ω_{rp} at high rotor speeds, D_T is plotted in Fig. 4 with the parameters of a 30 kW motor prototype. In this case, D_T has a great influence on the electromagnetic torque, which cannot be ignored. Therefore, the effects of φ_r should be considered to achieve a good control performance.

Due to the features of disturbance rejection, strong robustness, and fast responses, the sliding mode control is very suitable to tackle this problem; thus, a rotor speed controller based on ISMC is proposed here. In terms of the CW stator currents, PI controllers are sufficient to deal with the effects of φ_r, considering the high bandwidth and quick tracking capability of the inner-loop controller. To summarize, a double closed-loop control scheme based on the ISMC and PI control method is proposed in this paper, and the electromagnetic torque and reactive power are adjusted by the CW stator current. The specific details are described in the next part.

III. Control Scheme for the Brushless Doubly Fed Machine

In general, two control targets are established. One is the rotor speed when the BDFM is operated as a motor or the active power when the BDFM is operated as a generator; the other is the reactive power provided by the BDFM. In this paper, the BDFM motoring operation is studied, and the proposed method aims to control the rotor speed and reactive power.

A. Speed Control of the BDFM

1) Problem Formulation: In order to conveniently design the controller, the quantitative relationship between the electromagnetic torque and CW stator current i_{cq} is rewritten as

$$T_e = K_L i_{cq} - D_T \quad (19)$$

where, K_L is the accurate parameter that varies with the BDFM parameters, and $K_L = \frac{3M_p M_c(p_p+p_c)|\varphi_p|}{2(L_p L_r - {M_p}^2)}$.

Furthermore, because the accurate BDFM parameters are difficult to obtain, K_L calculated by (19) is inaccurate and is composed of two parts. One is calculated from the nominal value of parameters, and the other is obtained from the uncertain parts of parameters (M_p, M_c, L_p, and L_r). Accordingly, D_T is difficult to be fed forward completely because of the inaccurate parameters and variable values in (18).

Considering the above effects, the mechanical equation in (13) can be rewritten as

$$\frac{d\omega_r}{dt} = a_1 i_{cq} - a_2\omega_r - \frac{\hat{T}_L}{J_0} + D \quad (20)$$

where i_{cq} is the control input of the speed controller, and it correspondingly determines the speed tracking performance; $\widehat{T_L}$ is the measured load torque; D is expressed as $D = \Delta a_1 i_{cq} - \Delta a_2\omega_r - \frac{\Delta T_L + D_T}{J_0} - \Delta J\frac{d\omega_r}{dt}$, and represents the lumped uncertainties; $a_1 = K_{L0}/J_0$ and $a_2 = B_0/J_0$ are the coefficients of i_{cq} and ω_r, respectively; and the symbol "Δ" represents the corresponding parametric uncertainties.

2) Controller Design: The design of the sliding mode controller has two important steps—1) designing a switching surface on which the sliding motion will take place and 2) designing a control law to force the system state trajectories to reach and slide on the surface. Moreover, when sliding

is achieved and maintained, robustness against matched uncertainties is guaranteed.

In terms of the uncertain linear time invariant system described in (20), ISMC has no reaching phase, the sliding is enforced throughout the entire system response, and the sliding motion is invariant to matched uncertainties during the sliding mode [27]. Thus, an integral sliding mode surface is designed in this paper, which is expressed as

$$S_\omega = e_\omega + k\int_0^t e_\omega(\tau)\,d\tau \tag{21}$$

where e_ω is the rotor speed tracking error and is defined as $e_\omega = \omega_{\rm ref} - \omega_r$, k is a preset positive constant and it determines how quickly the error e_ω approaches zero once the state is on the surface.

For the sliding mode control method, the control input consists of two parts: one is the feedforward terms constructed by the measured variables and known parameters, denoted as the equivalent control, to maintain the sliding motion on the sliding surface; and the other is the control law designed to attenuate the effects of the system uncertainties, denoted as the switching control, which forces the system state on a suitably defined sliding manifold $S_\omega = 0$ in finite time. Thus, in order to make the differential of S_ω approach zero, the control input is designed as

$$\begin{aligned} i_{cq} &= {i_{cq}}^{\rm equ} + {i_{cq}}^{\rm SMC} \\ {i_{cq}}^{\rm equ} &= \frac{1}{a_1}\frac{d\omega_{\rm ref}}{dt} + \frac{a_2}{a_1}\omega_r + \frac{\hat{T}_L}{K_{L0}} + \frac{k}{a_1}e_\omega \\ {i_{cq}}^{\rm SMC} &= \frac{c}{a_1}{\rm sign}(S_\omega) \end{aligned} \tag{22}$$

where c is the control gain of the sliding mode controller, and it affects the amplitude of chattering. The criterion for the design of c is discussed next.

3) Reachability Condition: To ensure the speed tracking error state trajectories converge toward the sliding surface at each time instant, the reachability condition must be satisfied. The analysis based on the Lyapunov approach is, therefore, discussed.

Assumption 1: All the parameters in (19) are bounded as $K_{\min} \le \Delta K_L + K_{L0} \le K_{\max}$, $J_{\min} \le \Delta J + J_0 \le J_{\max}$, and $B_{\min} \le \Delta B + B_0 \le B_{\max}$.

Assumption 2: Considering the practical factors such as the mechanical inertia and the output capacity of the power converter, i_{cq}, φ_r, ω_r, and its differential $d\omega_r/dt$ are bounded, as well as external disturbance $\Delta T_{\rm L}$.

According to the assumptions above, although D is affected by the parameter variations and the operation state of the BDFM, it is bounded to a known non-negative value, denoted as $|D|$.

The Lyapunov function is defined as $V = S_\omega^2/2$, and the time derivative of V is calculated from (20)–(22), as

$$\begin{aligned} \frac{dV}{dt} &= S_\omega\frac{dS_\omega}{dt} = S_\omega\left(\frac{de_\omega}{dt} + ke_\omega\right) \\ &= S_\omega\left(-c\,{\rm sign}(S_\omega) - D\right) \\ &= -c|S_\omega| - DS_\omega \\ &\le (-c - D)|S_\omega|. \end{aligned} \tag{23}$$

In order to enforce a sliding mode, the value of the gain c should be greater than any disturbance or uncertainty in the system. Therefore, based on Assumption 1, any choice of c must satisfy $c \ge |D|$. In other words, the speed tracking error trajectory converges to the sliding surface $S_\omega = 0$ in infinite time, and remains on this surface when $c \ge |D|$ holds. When $S_\omega = 0$, $dS_\omega/dt = 0$, the tracking error e_ω exponentially converges to zero, according to (21), which is independent of the switching signal. According to the direct Lyapunov approach, V is positive definite, and dV/dt is negative definite when $c \ge |D|$. The origin is then globally asymptotically stable. That is, the stability is guaranteed with a suitable c, even when the parametric uncertainties and other system disturbances exist.

Finally, in order to overcome the chattering phenomenon around the sliding mode surface, the saturation function is utilized to replace the sign function in (22), and the command current $i_{cq\rm ref}$ for the speed tracking is calculated as

$$i_{cq\rm ref} = \frac{1}{a_1}\frac{d\omega_{\rm ref}}{dt} + \frac{a_2}{a_1}\omega_r + \frac{\hat{T}_L}{K_{L0}} + \frac{k}{a_1}e_\omega + \frac{c}{a_1}{\rm sat}(S_\omega) \tag{24}$$

where sat() represents the saturation function and is expressed as ${\rm sat}(S_\omega) = \begin{cases} {\rm sign}(S_\omega), & |S_\omega| > \varepsilon \\ \frac{S_\omega}{\varepsilon}, & \text{otherwise} \end{cases}$; and ε ($\varepsilon > 0$)is the range of the band.

B. Reactive Power Control of the BDFM

As discussed before, the reactive power is unaffected by the disturbance of φ_r in the steady state. Therefore, a PI controller can sufficiently compensate the tracking error caused by the unmatched parameters, and the controller parameters are minimal. In this case, the reference current i_{cd} contains the feedforward term, which is calculated by the nominal parameters and measured electrical variables, and the compensation term obtained from the PI controller. The reference current $i_{cd\rm ref}$ is then calculated as

$$\begin{aligned} i_{cd\rm ref} = {} & \frac{2\left(L_{r0}L_{p0} - {M_{p0}}^2\right)}{3|v_p|M_{p0}M_{c0}}Q_{p\rm ref} - \frac{L_{r0}}{M_{p0}M_{c0}}|\varphi_p| \\ & + \left(k_{pQ} + \frac{k_{iQ}}{s}\right)(Q_{p\rm ref} - Q_p) \end{aligned} \tag{25}$$

where k_{pQ} and k_{iQ} are the controller parameters.

C. Current Control of the BDFM

1) Structure of the CW Stator Current Controller: Controlling the CW stator current well is directly responsible for the electromagnetic torque production and the reactive power. The

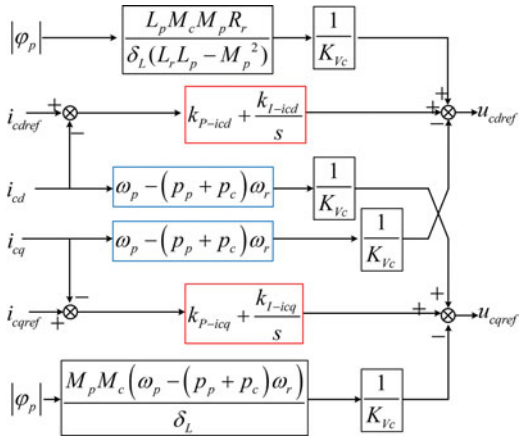

Fig. 5. CW stator current control diagram.

differential equations of the *dq* components of the CW stator current are calculated from (8), (9), and (11), and they are expressed as

$$\begin{aligned}\frac{di_{cd}}{dt} &= -K_{Ic}i_{cd} + K_{Vc}v_{cd} + D_{i_{cd}} + D_{\varphi_{rd}} \\ \frac{di_{cq}}{dt} &= -K_{Ic}i_{cq} + K_{Vc}v_{cq} + D_{i_{cq}} + D_{\varphi_{rq}}\end{aligned} \tag{26}$$

where $\delta_L = L_c L_p L_r - {M_c}^2 L_p - {M_p}^2 L_c$, K_{Ic} and K_{Vc} are the coefficients of the CW stator current and voltage; D_{icd} and D_{icq} are the coupling terms; $D_{\varphi rd}$ and $D_{\varphi rq}$ are the disturbances caused by the rotor flux, respectively. Moreover, they are expressed as follows:

$$\begin{aligned}K_{Ic} &= \frac{L_r L_p - {M_p}^2}{\delta_L} R_c + \frac{{L_p}^2 {M_c}^2}{\delta_L \left(L_r L_p - {M_p}^2\right)} R_r \\ K_{Vc} &= \frac{\left(L_p L_r - {M_p}^2\right)}{\delta_L} \\ D_{i_{cd}} &= \left(\omega_p - \left(p_p + p_c\right)\omega_r\right) i_{cq} - \frac{L_p M_c R_r M_p}{\delta_L \left(L_r L_p - {M_p}^2\right)} |\varphi_p| \\ D_{i_{cq}} &= -\left(\omega_p - \left(p_p + p_c\right)\omega_r\right) i_{cd} \\ &\quad + \frac{M_p M_c \left(\omega_p - \left(p_p + p_c\right)\omega_r\right)}{\delta_L} |\varphi_p| \\ D_{\varphi_{rd}} &= \frac{L_p M_c p_c \omega_r}{\delta_L} \varphi_{rq} + \frac{{L_p}^2 M_c R_r}{\delta_L \left(L_r L_p - {M_p}^2\right)} \varphi_{rd} \\ D_{\varphi_{rq}} &= \frac{L_p M_c p_c \omega_r}{\delta_L} \varphi_{rd} + \frac{{L_p}^2 M_c R_r}{\delta_L \left(L_r L_p - {M_p}^2\right)} \varphi_{rq}.\end{aligned} \tag{27}$$

As shown in (26), because the CW stator currents are measured and the PW stator flux is estimated, D_{icd} and D_{icq} are eliminated by a feedforward control. The PI control method is utilized to solve the first-order problems and compensate the effects of $D_{\varphi rd}$ and $D_{\varphi rq}$. The current control problems are then simplified as a common issue. The current control diagram is shown in Fig. 5, where the CW stator current references are obtained from (24) and (25). Furthermore, K_{P_icd}, K_{P_icq}, K_{I_icd}, and K_{I_icq} are the proportion coefficients and integral coefficients of the PI controllers, respectively.

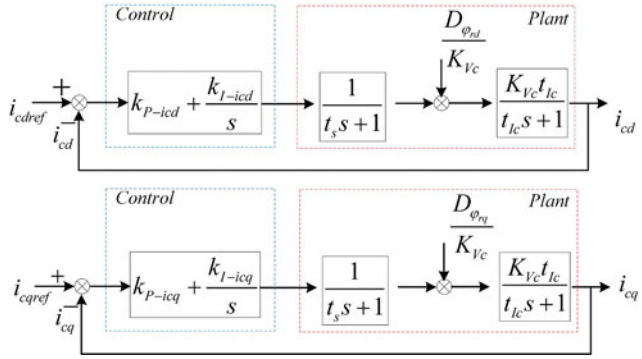

Fig. 6. Block diagram of the inner-loop system.

2) Design of the PI Controller: In order to simplify the analysis, the inverter is modeled as a first-order transfer function, where t_s is a smaller time constant composed of the inverter dead time, signal conditioning, analog-to-digital conversion, and processing time delays. When the cross terms are eliminated by a forward feedback control as shown in Fig. 5; the block diagram of the inner-loop system is simplified, as shown in Fig. 6, where t_{Ic} is the time constant of (26), calculated as $t_{Ic} = 1/K_{Ic}$, and $t_{Ic} > t_s$. It can be seen that i_{cd} and i_{cq} have the same subsystem structures. Moreover, the PI controllers are designed with the identical method, and the subsystem of i_{cq} is taken as an example here.

Typically, the PI controller is designed to cancel the inertia link with a larger time constant, the gain of the PI controller satisfies $K_{P\_icq} = t_{Ic} K_{I\_icq}$ according to Fig. 6, and the closed loop transfer function is simplified as

$$G_{oq} = \frac{\frac{K_{Vc} t_{Ic} k_{I-icq}}{s(t_s s+1)}}{1 + \frac{K_{Vc} t_{Ic} k_{I-icq}}{s(t_s s+1)}} = \frac{\frac{K_{Vc} t_{Ic} k_{I-icq}}{t_s}}{s^2 + \frac{1}{t_s} s + \frac{K_{Vc} t_{Ic} k_{I-icq}}{t_s}}. \tag{28}$$

As shown in (28), a standard second-order system is obtained. Designing a damping factor of $1/\sqrt{2}$, the integral coefficient is then selected as $K_{I\_icq} = 1/(2K_{Vc} t_s t_{Ic})$, in order to achieve the unit magnitude of the closed-loop frequency response with as large as possible a bandwidth, and to avoid a significant overshoot [28].

D. Proposed Control System and Its Stability Discussion

In conclusion, the control scheme based on the PW stator flux orientation frame is developed as shown in Fig. 7. The outer-loop control is constructed by an ISMC speed controller and a PI reactive power controller, and the inner-loop control consists of two PI current controllers. The proposed method simultaneously achieves the rotor speed control and reactive power adjustment. In this method, three PI controllers are utilized, and the bandwidth of the inner-loop controller is designed to be larger than that of the outer-loop controller. The selections of the PI controller parameters have been discussed in Sections B and C.2 in part III, which have provided theoretical guidance for the simulations and experiments.

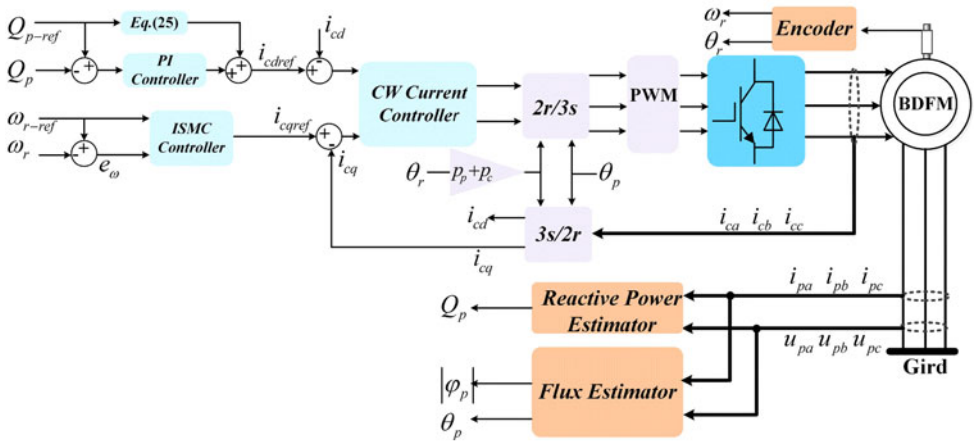

Fig. 7. Block diagram of the proposed vector control scheme.

The system stability is difficult to directly analyze, due to the combined control scheme of the ISMC and PI control methods. According to (20) and (26), the BDFM system is a two-time scale model, and $a_1 \ll K_{Ic}$. Furthermore, (20) is then a slow model. In this case, two steps are discussed using the singular perturbation theory to study the system stability.

Step 1: For the outer-loop, the time scale of the rotor speed is larger than that of the currents, and it tracks the reference in a small-time scale. Therefore, i_{cq} could be directly treated as a control input; thus, the order of the system is reduced. The stability of the subsystem (20) is then guaranteed by the direct Lyapunov approach method, which has been discussed in Section A. 3).

Step 2: The precondition for i_{cq} being treated as a control input is that the current loop is well designed and stable. To prove the stability of the current loop, it is reasonable to treat the speed as a constant in the current time scale. The stability is then analyzed using a small signal model. In Fig. 6, the closed-loop transfer function of the subsystem of i_{cq} is expressed as

$$G_{coq} = \frac{\frac{K_{Vc}t_{Ic}\left(k_{P-icq}s+k_{I-icq}\right)}{s(t_s s+1)(t_{Ic}s+1)}}{1+\frac{K_{Vc}t_{Ic}\left(k_{P-icq}s+k_{I-icq}\right)}{s(t_s s+1)(t_{Ic}s+1)}} = \frac{K_{Vc}t_{Ic}\left(k_{P-icq}s+k_{I-icq}\right)}{t_s t_{Ic}s^3+\left(t_{Ic}+t_s\right)s^2+\left(1+K_{Vc}t_{Ic}k_{P-icq}\right)s+K_{Vc}t_{Ic}k_{I-icq}}. \quad (29)$$

According to the Routh stability criterion, the stability of the subsystem (29) is guaranteed by $K_{I\_icq} > 0$ and $k_{P-icq} > \frac{t_s t_{Ic} k_{I-icq}}{t_{Ic}+t_s} - \frac{1}{K_{Vc}t_{Ic}}$, which is easy to achieve, since $\frac{t_s t_{Ic}}{t_{Ic}+t_s}$ is very small.

IV. Simulation and Experimental Results

A. System Configuration

In this part, the simulation and experimental platforms of a BDFM system are built with the motor parameters listed in Table I. The PW stator of the BDFM is directly connected to the grid, and the CW stator of the BDFM is fed by a back-to-back PWM converter. In the experiments, the BDFM is mechanically coupled with a 30-kW induction machine that works as a load machine as shown in Fig. 8. A magneto-electric phase difference torque sensor JC2C is used to monitor the torque. Speed and position signals are obtained from an incremental encoder, E6B2-CWZ6C provided by OMRON, with a resolution of 2000 pulses/*r*. The control method is realized by a combination of a digital signal processor TM320F28335 and a field-programmable gate array EP2C8T144C8N.

In order to examine the control performance of the proposed method, several experimental scenarios are tested using the MATLAB/Simulink platform and the experimental platform. As previously discussed, the parameters of current PI controllers are designed with reference to the common first-order system, and the parameters in the discrete PI controllers are $K_{P\_icd} = K_{P_{icq}} = 1.3$, $K_{I\_icd} = K_{I\_icq} = 15$, whereas the

TABLE I
Parameters of the BDFM

Parameters	Value
Rated power (kW)	30
Rated voltage (V)	380
Pole-pairs of the PW stator	1
Pole-pairs of the CW stator	3
Resistance of the PW stator (Ω)	0.403
Resistance of the CW stator (Ω)	0.343
Resistance of rotor (Ω)	0.785
Self-inductance of the PW stator (H)	0.710
Self-inductance of the CW stator (H)	0.061
Self-inductance of the rotor (H)	0.787
Mutual inductance of the PW stator (H)	0.706
Mutual inductance of the CW stator (H)	0.059

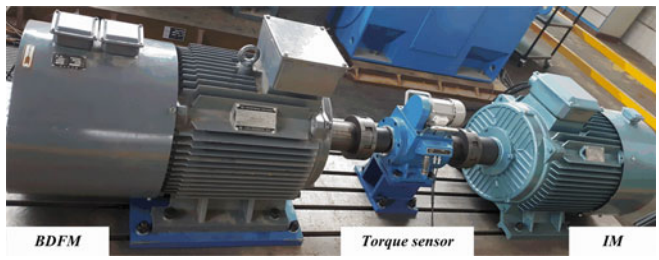

Fig. 8. Experimental platform.

PI controller of the reactive power slightly adjusts its tracking performance, and the gains are $K_{pQ} = 0.05$ and $K_{Iq} = 0.1$.

B. Simulation Results

In the simulations, two cases are studied to evaluate the control performance of the proposed method. The first case is the comparative analysis between the proposed method and a PI control method. The selection of PI parameters influences the control performance of the PI controller, and different static and dynamic responses are obtained with different parameters. In this case, the PI parameters are obtained from a universal design criterion as mentioned in Section C in part III, and the comparative analyses are conducted. The second case is the system response of the proposed method with different modeling parameters. Moreover, because the effects of φ_r increase with a high rotor speed, the ISMC gain c varies with the rotor speed. Furthermore, the load torque is 100 N·m. Considering the disturbance of the load torque and parametric errors, the parameters of the ISMC controller are set as: $k = 20$, $c = 35\ \omega_p/\omega_{rp}$, and $\varepsilon = 0.2$.

Case 1: Fig. 9 shows waveforms of the rotor speed, electromagnetic torque, reactive power of PW stator, and CW stator currents, with the proposed method and PI method, respectively; where the output of the PI controller is fed into a saturation block. The reference rotor speeds are 450, 850, 1000, 1300, and 1600 r/min, which correspond to the changing times $t = 2$ s, $t = 5$ s, $t = 8$ s, and t = 11 s, respectively. As shown in Fig. 9, the rotor speed and reactive power track the references quickly with the ISMC method. Moreover, the rise time is smaller than 1.2 s, the steady-state errors of the rotor speed and reactive power are ± 0.5 r/min and ± 50 Var, and the BDFM works from the subsynchronous mode to the super-synchronous mode with a satisfactory dynamic response with the ISMC method. When the reference rotor speed is 1600 r/min, there are some fluctuations in the dynamic state, but the BDFM system also achieves a good steady performance.

In addition, when the rotor speed is near the nature speed, such as 850 and 1000 r/min, an acceptable control performance is achieved with the PI method, as shown in Fig. 9. However, a large steady-state error of ± 1.5 r/min is obtained when the rotor speed is 450 r/min. In particular, when the rotor speed is 1600 r/min, the BDFM system is unstable with the PI method, which is caused by the increasing value of D_{T}, and the CW stator currents are uncontrollable.

Compared with the ISMC method, the transient tracking performance is worse with the PI method, the rise time increases, as well as the transient values of CW stator currents. Moreover, the electromagnetic torque and reactive power have large pulsations as a result.

Thus, it can be seen from Fig. 9 that the proposed ISMC method achieves a good control performance in a wide rotor speed range.

Case 2: In practice, motor parameters are difficult to obtain precisely, which also change with the temperature and the motor working occasions. From (19), the mutual inductance M_p and M_c directly affect the selections of controller parameters; thus,

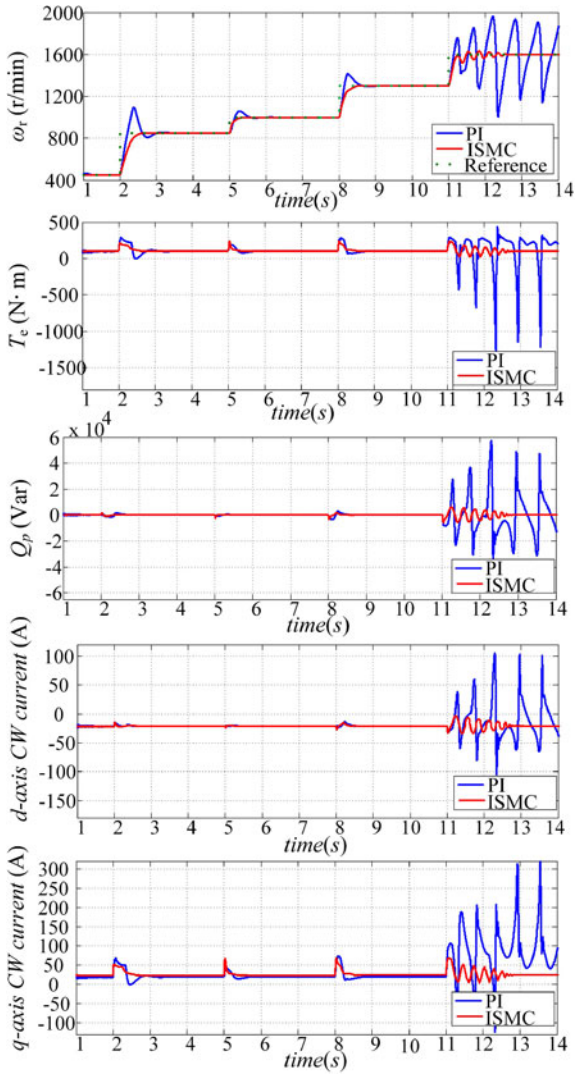

Fig. 9. Simulation results with the proposed method and PI method.

the robustness of the proposed method is tested with ±40% mutual inductance variations, and the simulation results are shown in Fig. 10.

In Fig. 10(a), when the mutual inductance M_c has ±40% errors from the nominal value, the waveforms of the rotor speed, electromagnetic torque, reactive power, and CW stator currents are shown from the top to the bottom, where MC represents the case that M_c is the nominal value; the MCI represents the case that M_c is 40% larger than the nominal one; and MCII represents the case wherein M_c is 40% smaller than the nominal value. With the parametric variations, the control performance of the BDFM system slightly decreases. The rise time increases with MCI and MCII, but the tracking performances are both acceptable. In MCI, the parametric error results in higher chattering when the rotor speed is 1300 r/min, especially the reactive power. In MCII, a stable operation is guaranteed with small tracking errors at 1300 r/min.

Fig. 10(b) shows the waveforms of the rotor speed, electromagnetic torque, reactive power, and CW stator currents when the mutual inductance M_p has ±40% variations; where MP,

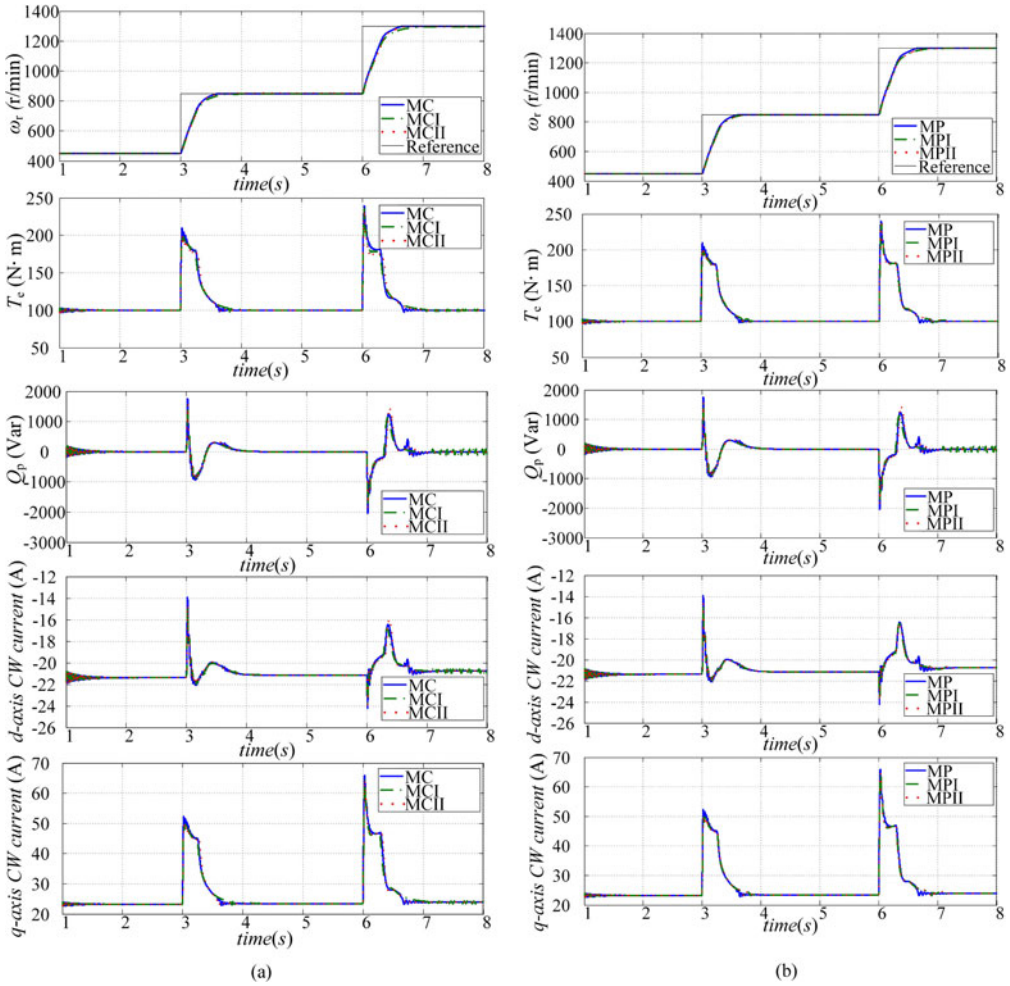

Fig. 10. Simulation results with different parameter errors. (a) Simulation results with $\pm 40\%$ M_c. (b) Simulation results with $\pm 40\%$ M_p.

MPI, and MPII represent the cases wherein M_p is the nominal value, and M_p is 40% larger and 40% smaller than the nominal value, respectively. It can be seen that the proposed methods with 40% M_p errors have worse steady and dynamic control performances than the case that M_p is the nominal value. Nonetheless, the tracking performances of the rotor speed are both satisfactory with quick tracking processes. However, the waveforms of the electromagnetic torque and reactive power have large fluctuations at high rotor speeds in MPI, as well as in MCI.

In conclusion, the control performance worsens when the parametric error exists. The waveforms in the steady state and in the dynamic state are both affected to some extent, and the effects with larger parametric errors are severe on the control system. According to (19) and (23), a larger c is required to achieve robust stability with larger parametric errors, especially when the rotor speed is high. As a result, the chattering may unavoidably increase.

C. Experimental Results

Case 1: In Fig. 11(a)–(c), the expected reactive power is 0 Var, and the reference rotor speeds are 450, 750, and 1100 r/min. Moreover, the BDFM works in the subsynchronous mode, synchronous mode, and super-synchronous mode, respectively. Meanwhile, the rotor speeds 450 and 1100 r/min are both out of the range by $\pm 30\%$ around the natural speed.

It can be seen that the rotor speed tracks the reference value well, and the tracking error is within about ± 2 r/min. Although the rotor speeds have some oscillations, the results are acceptable in practical applications. In addition, this error range can be adjusted by the band range ε. The reactive power fluctuates by about ± 400 Var at different rotor speeds, and the errors are large at high rotor speeds, due to the large effects caused by the rotor speed.

In Fig. 11(d), the expected reactive power is 5000 Var at 800 r/min, and the reference reactive power tracks the reference with some fluctuations. In the steady state, i_{cd} increases accordingly to generate the expected reactive power at the PW stator, whereas i_{cq} is unchanged and maintains the proper electromagnetic torque. In conclusion, the proposed method adjusts the rotor speed and the reactive power independently, and it achieves a good steady-state performance. Furthermore, the CW stator currents are stable at a certain value with tiny fluctuations. In this method, i_{cq} relates to the electromagnetic torque, whereas i_{cd} corresponds to the reactive power. When the reactive power is zero, i_{cd} is mainly used to establish the PW stator flux, and

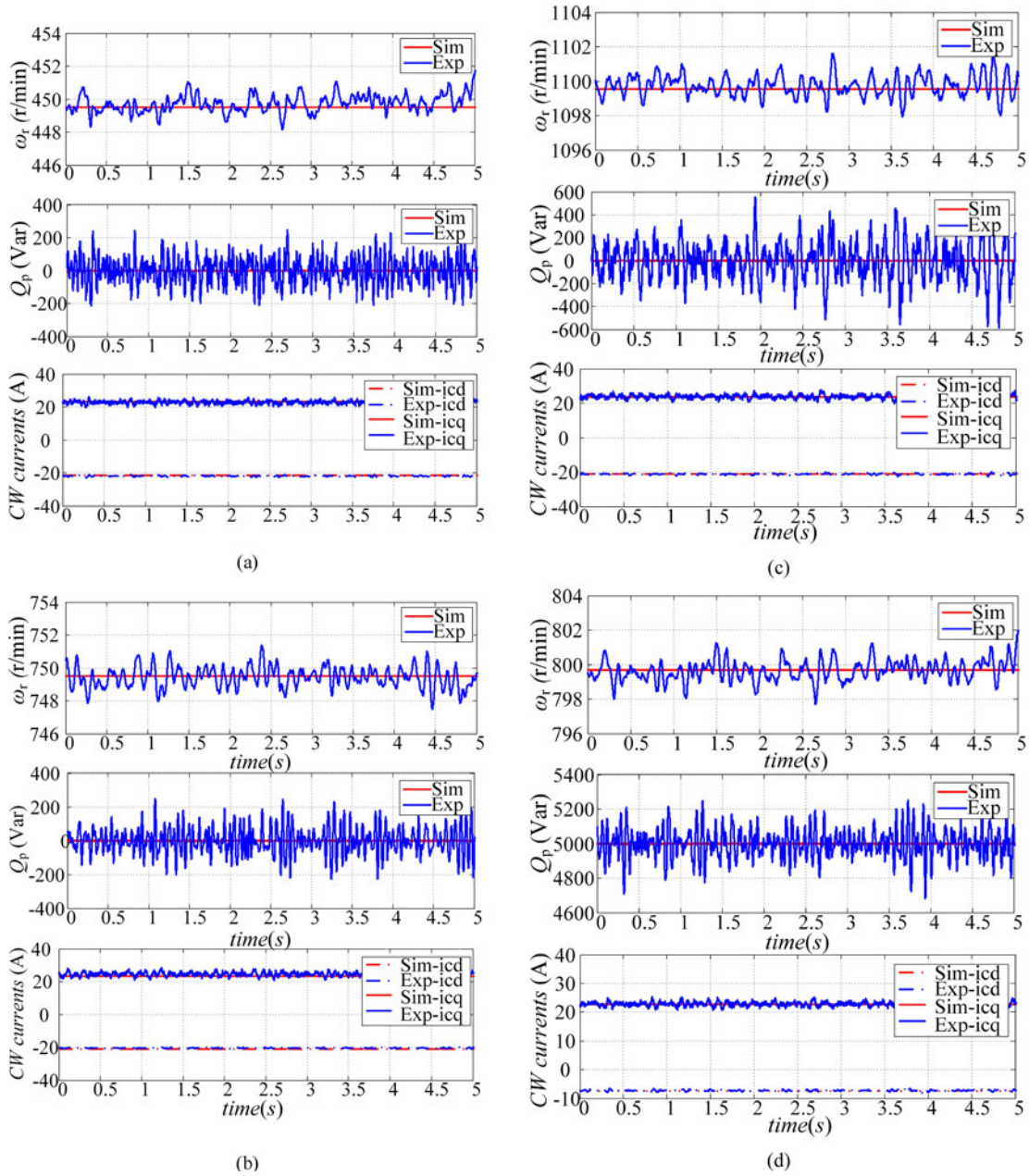

Fig. 11. Simulation and experimental results at different rotor speeds. (a) $\omega_r = 450$ r/min. (b) $\omega_r = 750$ r/min. (c) $\omega_r = 1100$ r/min. (d) $Q_p = 5000$ Var.

it is determined by the grid. Compared with the simulation results in Fig. 11, the tracking error is relatively large, due to the nonidealities of the power source and IGBT switches in the experiments.

Case 2: In general, the rotor speed is variable in practical applications, and the dynamic performance is critically important. Therefore, the dynamic experiments are conducted in this case; two tests about the changes of the reference rotor speed and load torque with the proposed method are considered. Fig. 12 illustrates the simulation and experimental results from a change in the command rotor speed and load torque.

In Fig. 12(a), the reference rotor speed of the BDFM changes from 600 to 850 r/min, and the BDFM works from the subsynchronous mode to the super-synchronous mode. The rise time is approximately 1.2 s, which is able to be adjusted by the controller parameters k and c, and the maximum limit of the CW stator current. On the other hand, the actual rotor speed tracks the reference well, the q-axis component of the CW stator current increases accordingly to generate a high electromagnetic torque during the acceleration process, and i_{cd} has a smooth transition when the rotor speed changes. However, both currents exhibit a tendency toward stabilization after the acceleration process.

In Fig. 12(b), the load torque changes from 100 to 50 N·m. Moreover, the rotor speed increases because the electromagnetic torque is larger than the load torque at the changing moment, and the rotor speed experiences a recovery process when the electromagnetic torque gradually decreases with the decrease of i_{cq}. Although the rotor speed has small fluctuations during

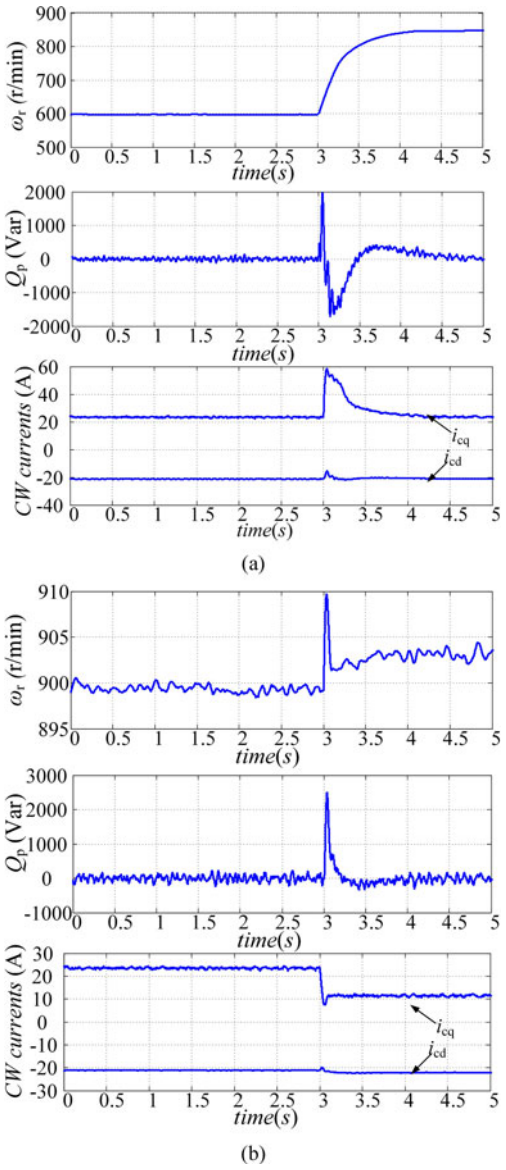

Fig. 12. Experimental results when the rotor speed changes. (a) Rotor speed changes from 600 to 850 r/min. (b) Load torque changes from 25 to 110 N·m.

the transience, it is able to track the reference value again, as displayed. Furthermore, i_{cq} then reaches a low value in the steady state. On the other hand, i_{cq} keeps the value after small variations, in order to maintain the reactive power constant. In conclusion, the proposed method can achieve good dynamic control performance.

V. Conclusion

In this paper, the mathematical model of the BDFM is discussed by taking the rotor flux as a disturbance. A robust control method based on ISMC is then proposed in the PW flux orientation frame. The developed method regulates the rotor speed and the reactive power of the PW stator with high steady-state accuracy, by compensating the effects of the rotor flux and parameter perturbation. Moreover, it guarantees the normal operation of the BDFM at different working modes. Furthermore, the steady-state performance and the dynamic tracking performance are good. The detailed experimental results on the BDFM bench verify the feasibility and correctness of the proposed method. Thus, this paper is greatly significant for the development of BDFM control methods.

References

[1] Z. Chen, J. M. Guerrero, and F. Blaabjerg, "A review of the state of the art of power electronics for wind turbines," *IEEE Trans. Power Electron.*, vol. 24, no. 8, pp. 1859–1875, Aug. 2009.

[2] F. Xiong and X. Wang, "Design of a low-harmonic-content wound rotor for the brushless doubly fed generator," *IEEE Trans. Energy Convers.*, vol. 29, no. 1, pp. 158–168, Mar. 2014.

[3] M. S. Boger, A. K. Wallace, and R. Spee, "Investigation of appropriate pole number combinations for brushless doubly fed machines applied to pump drives," *IEEE Trans. Ind. Appl.*, vol. 31, no. 5, pp. 1022–1028, Jan. 1996.

[4] R. A. McMahon, X. Wang, E. Abdi-Jalebi, P. J. Tavner, P. C. Roberts, and M. Jagiela, "The BDFM as a generator in wind turbines," in *Proc. 12th Int. Power Electron. Motion Control Conf.*, 2006, pp. 1859–1865.

[5] P. C. Roberts, "A study of brushless doubly-fed (induction) machines," Ph. D. dissertation, Emanuel College, Cambridge Univ., Cambridge, U.K., 2004.

[6] D. Zhou, R. Spee, and A. K. Wallace, "Laboratory control implementations for doubly-fed machines," in *Proc. IEEE Int. Conf. Ind. Electron., Control, Instrum.*, 1993, pp. 1181–1186.

[7] J. Pozal, E. Oyarbide, D. Roye, and I. Sarasolal, "Stability analysis of a BDFM under open-loop voltage control," in *Proc. 11th Eur. Conf. Power Electron. Appl.*, 2005, pp. 1–10.

[8] I. Sarasola, J. Poza, E. Oyarbide, and M. A. Rodriguez, "Stability analysis of a brushless doubly-fed machine under closed loop scalar current control," in *Proc. IEEE 32nd Annu. Conf. Ind. Electron. Soc.*, 2006, pp. 1527–32.

[9] R. A. McMahon, P. C. Roberts, X. Wang, and P. J. Tavner, "Performance of BDFM as generator and motor," *IEE Proc. Elect. Power Appl.*, vol. 153, no. 2, pp. 289–299, Mar. 2006.

[10] S. Y. Shao, E. Abdi, and R. A. McMahon, "Low-cost variable speed drive based on a brushless doubly-fed motor and a fractional unidirectional converter," *IEEE Trans. Ind. Electron.*, vol. 59, no. 1, pp. 317–325. Jan. 2012.

[11] Y. Liu, A. Wu, B. Chen, K. Chen, and G. luo, "Control design and experimental verification of the brushless doubly-fed machine for stand-alone power generation applications," *IET Electr. Power Appl.*, vol. 10, no. 1, pp. 25–35, Jan. 2016.

[12] W. R. Brassfield, R. Spee, and T. G. Habetler, "Direct torque control for brushless doubly-fed machines," *IEEE Trans. Ind. Appl.*, vol. 32, no. 5, pp. 1098–1104, Sep./Oct. 1996.

[13] I. Sarasola, J. Poza, M. A. Rodriguez, and G. Abad, "Direct torque control design and experimental evaluation for the brushless doubly fed machine," *Energy Convers. Manag.*, vol. 52, no. 2, pp. 1226–1234, 2011.

[14] A. Zhang, X. Wang, W. Jia, and Y. Ma, "Indirect stator-quantities control for the brushless doubly fed induction machine," *IEEE Trans. Power Electron.*, vol. 29, no. 3, pp. 1392–1401, Mar. 2014.

[15] B. Hopfensperger, D. J. Atkinson, and R. A. Lakin, "Stator flux oriented control of a cascaded doubly-fed induction machine," *IEE Proc. Elect. Power Appl.*, vol. 146, no. 6, pp. 597–605, Nov. 1999.

[16] D. Zhou, R. Spee, and G. C. Alexander, "Experimental evaluation of a rotor flux oriented control algorithm for brushless doubly-fed machines," *IEEE Trans. Power Electron.*, vol. 12, no. 1, pp. 72–78, Jan. 1997.

[17] B. Hopfensperger, D. J. Atkinson, and R. A. Lakin, "Combined magnetizing flux oriented control of the cascaded doubly-fed induction machine," *IEE Proc. Electr. Power Appl.*, vol. 148, no. 4, pp. 354–362, Jul. 2001.

[18] S. Shao, A. Ehsan, B. Farhad, and M. Richard, "Stator-flux-oriented vector control for brushless doubly fed induction generator," *IEEE Trans. Ind. Electron.*, vol. 56, no. 10, pp. 4220–4228, Oct. 2009.

[19] J. Poza, E. Oyarbide, I. Sarasola, and M. Rodriguez, "Vector control design and experimental evaluation for the brushless doubly fed machine," *IET Elect. Power Appl.*, vol. 3, no. 4, pp. 247–256, Jul. 2009.

[20] J. Poza, E. Oyarbide, D. Roye, and M. Rodriguez, "Unified reference frame dq model of the brushless doubly fed machine," *IEE Proc. Electr. Power Appl.*, vol. 153, no. 5, pp. 726–734, Sep. 2006.

[21] R. Cárdenas, R. Peña, P. Wheeler, J. Clare, A. Muñoz, and A. Sureda, "Control of a wind generation system based on a brushless doubly-fed induction generator fed by a matrix converter," *Electric Power Syst. Res.*, vol. 103, pp. 49–60, Oct. 2013.
[22] J. Chen, W. Zhang, B. Chen, and Y. Ma, "Improved vector control of brushless doubly fed induction generator under unbalanced grid conditions for offshore wind power generation," *IEEE Trans. Energy Convers.*, vol. 31, no. 1, pp. 293–302, Mar. 2016.
[23] L. J. Hunt, "A new type of induction motor," *J. Inst. Electr. Eng.*, vol. 39, pp. 648–677, 1907.
[24] G. Esfandiari, M. Ebrahimi, A. Tabesh, and M. Esmaeilzadeh, "Dynamic modeling and analysis of cascaded DFIMs in an arbitrary reference frame," *IEEE Trans. Energy Convers.*, vol. 30, no. 3, pp. 999–1007, Sept. 2015.
[25] J. Hu and B. Wu, "New integration algorithms for estimating motor flux over a wide speed range," *IEEE Trans. Power Electron.*, vol. 13, no. 5, pp. 969–977, Sep. 1998.
[26] S. Tohidi, "Analysis and simplified modelling of brushless doubly-fed induction machine in synchronous mode of operation," *IET Electr. Power Appl.*, vol. 10, no. 2, pp. 110–116, 2016.
[27] M. Rubagotti, A. Estrada, F. Castanos, and F. Leonid, "Integral sliding mode control for nonlinear systems with matched and unmatched perturbations," *IEEE Trans. Autom. Control*, vol. 56, no. 11, pp. 2699–2704, Nov. 2011.
[28] C. Rabelo, W. Hofmann, J. L. da Silva, R. G. de Oliveira, and S. Silva, "Reactive power control design in doubly fed induction generators for wind turbines," *IEEE Trans. Ind. Electron.*, vol. 56, no. 10, pp. 4154–4162, Oct. 2009.

Guanguan Zhang received the B.S. degrees in automation from the School of Information Science and Engineering, Central South University, and she is currently working toward the Ph.D. degree in power electronics and power transmission from the School of Information Science and Engineering, Central South University.

She is currently a joint Ph.D. student supported by the China Scholarship Council in the Department of Energy Technology, Aalborg University, Aalborg, Denmark, where she focuses on the reliability analysis of wind power system. Her research interests include matrix converter, motor control, and wind power system.

Jian Yang (M'09) received the Ph.D. degree in electrical engineering from the University of Central Florida, Orlando, FL, USA, in 2008.

He was a Senior Electrical Engineer with Delta Tau Data Systems, Inc., Los Angeles, CA, USA, from 2007 to 2010. Since 2011, he has been with Central South University, Changsha, China, where he is currently an Associate Professor in the School of Information Science and Engineering. His main research interests include control application, motion planning, and power electronics.

Yao Sun (M'13) was born in Hunan, China, in 1981. He received the B.S. degree in automation, the M.S. and Ph.D. degrees in electric engineering from the School of Information Science and Engineering, Central South University, Changsha, China, in 2004, 2007, and 2010, respectively.

Since 2013, he has been an Associate Professor in the School of Information Science and Engineering, Central South University. His research interests include matrix converter, microgrid, and wind energy conversion system.

Mei Su was born in Hunan, China, in 1967. She received the B.S. degree in automation, M.S., and Ph.D. degrees in electric engineering from the School of Information Science and Engineering, Central South University, Changsha, China, in 1989, 1992, and 2005, respectively.

Since 2006, she has been a Professor in the School of Information Science and Engineering, Central South University. Her research interests include matrix converter, adjustable speed drives, and wind energy conversion system.

Weiyi Tang was born in Jiangsu, China, in 1991. He received the B.S. degree in automation from the Central South University, Changsha, China, in 2013, where he is working toward the Ph.D. degree in control science and engineering.

His research interest focuses on motor contro**l.**

Qi Zhu was born in Anhui Province, China, in 1993. He received the B.S. degree in electrical engineering and automation from the Central South University, Changsha, China, in 2014, where he is currently working toward the Ph.D. degree in electrical engineering.

His research interests include matrix converters and wireless power transfer.

Hui Wang received the B.S. degree in automation, the M.S., and Ph.D. degrees in electric engineering from the School of Information Science and Engineering, Central South University, Changsha, China, in 2008, 2011, and 2014, respectively.

Since 2016, he has been in the School of Information Science and Engineering, Central South University. His research interests include matrix converter, dc/dc converters, and solid-state transformer.